Chapter

The Influences of Combined Distortions on Fan Performance

Xu Quanyong, Wu Honghu and Hou Anping

Abstract

Combined distortions negatively affect the aerodynamic stability of fans, but previous studies have limitations. The 3D CFD method was used to calculate the aerodynamic stability of fans under the total pressure and swirl distortion, total temperature and swirl distortion, and total pressure and total temperature distortion in the work. Rotor 67 was taken as the research object. According to the calculation results, the influences of variable distortion parameters on fan performance under combined distortions were summarized to establish the functional relationship between stability margin losses and distortion parameters.

Keywords: combined distortion, stall, aerodynamic performance, fan, aero engine

1. Introduction

The inlet distortion is a common phenomenon in takeoff and flight. Some specific conditions, such as takeoff, aircraft inhaling missile exhausts, and aircraft use of the S-duct inlet, may lead to combined distortions at the aero-engine inlet, including the total pressure distortion, total temperature distortion, and swirl distortion. The inlet distortion negatively affects aero-engine performance, which directly threatens aero-engine stability and safety. Therefore, it is necessary to study the influences of combined distortions on aero-engine stability.

Researchers have studied the influences of combined distortions on the stability of the engine compression system for many years. They focus on the total pressure and total temperature distortion instead of other combined distortions. Braithwaite and Braithwaite *et al.* obtained the operating parameters of the engine under the 180° total pressure and total temperature distortion in different phases by testing engines TF30-P-3 and YTF34. The pressure distortion required to stall the compressor increases as the temperature distortion decreases for aligned high temperatures and low pressures. The required pressure distortion increases with the increased temperature distortion for the opposed high-temperature low-pressure case. The most persistent distortion occurs when the high temperature and low pressure are in the same 180° sector; the distortion attenuates the most when the low-pressure zone is opposite to the high-temperature zone [1, 2].

Mehalic studied the temperature and pressure distortion of the engine by testing engine PW1128. When the low-pressure zone coincides with the high-temperature

zone, it will cause the high-pressure compressor to stall. When the low-pressure zone is opposite to the high-temperature zone, the influence on the stability of the high-pressure compressor will be weakened [3]. Davis used a stage-by-stage parallel compression system simulation and found the largest loss in stall-margin results under the steady-state pressure and temperature distortion when the high-temperature and low-pressure regions coincide. The stability limit has been lowered for the steady-state pressure distortion and temperature ramps. Stability is related to the position of the time for the dynamic combined distortion of the pressure oscillation and temperature gradient (the linear increase of temperature over time) when the temperature gradient is applied in the pressure oscillation cycle [4]. Modified parallel compressor theory can simulate more complex distortion patterns, including temperatures, pressures, and swirls. However, radial distortion effects cannot be included easily due to the changes in radial work distributions [5].

Frohnapfel *et al.* conducted experimental investigations and found that it is impossible to completely decouple total pressure and swirl distortions. A total pressure distortion typically creates a secondary flow field as air mixes from high to low-pressure regions within the distortion. Similarly, flow losses of axial flow at the inlet associated with turning under the swirl distortion for swirl distortion testing disturb the flow pressure field. The radial and tangential flow angles at the fan outlet are significantly influenced by the inlet-swirl distortion; whereas, the total and static pressure ratios of the fan are significantly influenced by the total pressure distortion at the inlet [6].

Huang found that the effect of combined distortions on engine stability is a complex nonlinear relationship rather than a simple addition of pressure and temperature distortion effects [7]. Ye *et al.* found that a compressor system creates maximum stability margin degradation when pressure distortion and temperature distortion phases coincide based on the numerical simulations of the 2D Euler equation, and the stability margin can be improved in some phases if a combined-distortion phase is changed suitably [8]. Xie *et al.* used the parallel compressor method and found that the influence of combined distortions on the fan and compressor pressure ratio is the same as that of the single-pressure distortion [9].

The parallel compressor model is often used in studying combined distortion. Pearson and McKenzie first proposed the parallel compressor theory in 1959 [10]. Reid [11], Mazzawy [12], and other researchers supplemented the model [13]. The theory shows that a compressor under the distortion can be treated as two or more sub compressors operating in parallel, and different levels of pressure- or temperature-distortions may be imposed upon their inlets, e.g., some take in distorted/undistorted air. Each sub compressor is assumed to operate independently of the other sub compressor except for the exit boundary where either a uniform static pressure or a uniform Mach number is imposed. As a result, each segment of the total system simulation will operate as a separate compression system. The entire compression system is considered to be unstable when one sub-compressor reaches the stability limit in this classical form. The mean operating point at instability is a weighted average of the low flow sector operating at the uniform flow stability boundary and the high flow sector operating at some other points far from the stability limit using the approach (see **Figure 1**) [14].

Research on the influences of combined distortions on the stability of the aero-engine compression system mainly adopts the parallel compressor method and the penetrating force method. However, the 3D computational fluid dynamics (CFD) numerical simulation is rarely used. Besides, research on combined distortions focuses

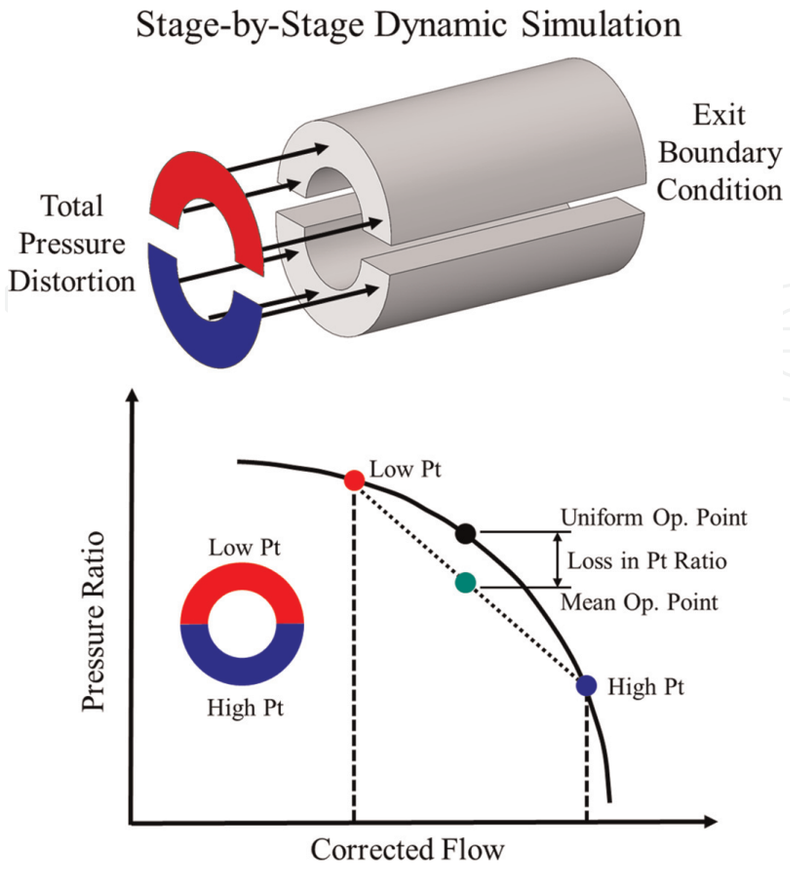

Figure 1.
Parallel compressor theory [14].

on the total pressure and total temperature distortion instead of combined distortions including the swirl distortion. The 3D CFD method was utilized to simulate the whole circumference of the rotor and study the influences of combined distortions on fan performance in the work. Valuable results were obtained.

2. Definition of inlet distortion parameters

The total pressure distortion, total temperature distortion, and swirl distortion parameters selected in the numerical simulation are as follows.

1. Steady-state circumferential-distortion parameter $\Delta\bar{\sigma}_0$ is selected as the total pressure distortion parameter. The index is the relative difference between the average total pressure recovery coefficient on the air interface plane (AIP) and the average total pressure recovery coefficient in the low-pressure zone. The low-pressure zone refers to the circumference range where the total pressure is less than the average total pressure on the AIP. The total pressure recovery coefficient is the ratio of the measured total pressure to the total pressure of undisturbed airflow before the inlet. The parameter is obtained by

$$\Delta\bar{\sigma}_0 = 1 - \frac{\sigma_0}{\sigma_{av}} \tag{1}$$

where σ_0 is the average total pressure recovery coefficient in the low-pressure region; σ_{av} the face-average total pressure recovery coefficient at the AIP.

1. Relative increase of average surface temperature δT_{2FAV} is selected as the total temperature distortion parameter. It numerically represents the temperature-distortion amplitude. The parameter is obtained by Eq. (2).

$$\delta T_{2FAV} = \frac{\Delta T_{2FAV}}{T_0} \tag{2}$$

where $\Delta T_{2FAV} = T_{2FAV}\text{-}T_0$ is the increase of the face-average total temperature, K; T_{2FAV} the face-average total temperature, K; T_0 the total temperature of the external test environment, K.

2. $\overline{\tau}_{87}$ is selected as the swirl distortion parameter. According to the preliminary calculation results, the inlet vortex is mainly the bulk swirl under the swirl distortion. $\overline{\tau}_{87}$ is the average τ_{87} value, which can represent overall vortex (bulk swirl) strength; τ_{87} is the ratio of the tangential component velocity at a radius of 0.87 R_{max} to the axial flow rate. τ_{87} is the tangent of airflow tangential angle δ and is often directly expressed by the airflow tangential angle. **Figure 2** shows the installation of the τ_{87} detector and defines the tangential angle of airflow [15].

The parameter is obtained by

$$\tau_{87} = \frac{v_t}{u} = \tan\delta \approx \delta \tag{3}$$

where u is the axial velocity, m/s; v_t the tangential velocity, m/s;

3. Stability margin. We choose the stability margin evaluated at a constant corrected rotor speed (see Eq. (4)).

$$SM = \left[\frac{\left(\pi_c/W_{a,c}\right)_{Su}}{\left(\pi_c/W_{a,c}\right)_o} - 1\right] \times 100\% \tag{4}$$

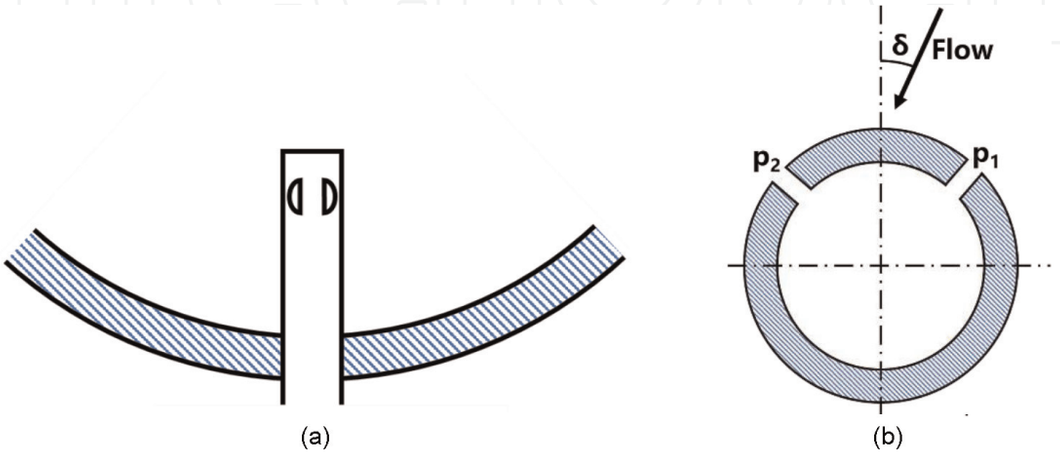

Figure 2.
Definition of τ_{87} [15]. (a) Installation of the τ_{87} detector. (b) Definition of the airflow tangential angle.

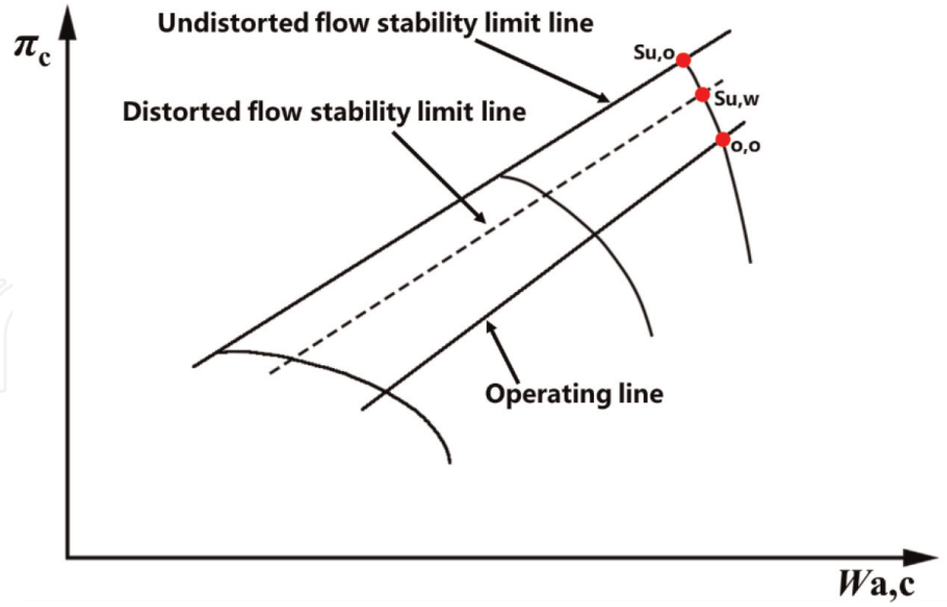

Figure 3.
Stability margin definition.

where *Su* is the stability-limit point, and *o* the operating point.
The stability margin loss is obtained by

$$\Delta SM_{Su,i} = SM_{Su,o} - SM_{Su,w} \tag{5}$$

where *Su, w* is distorted flow, and *Su, o* is undistorted flow (clean flow).
Figure 3 shows the parameters in the definition of the stability margin loss.

3. Numerical simulation method

The numerical simulation of aircraft outflow is performed. The outlet section of the inlet duct in the aircraft outflow calculation results is taken as the inlet section in the internal-flow calculation of the compressor. Then, total pressure, total temperature, velocity component, and other gas parameters on the inlet section in the compressor are obtained by interpolation and combination according to the calculation conditions. Finally, the function of the stability margin loss and distortion parameters is established based on the calculation results.

The selected research object is NASA Rotor 67. Rotor 67 is a low-aspect-ratio transonic axial-flow fan rotor designed by NASA Lewis Research Center. The geometry of Rotor 67 and the experimental data obtained using both aerodynamic probes and laser anemometer measurements were reported by Strazisar *et al.* [16]. **Figure 4** shows the meridional view and 3D model of Rotor 67, and **Table 1** lists basic design specifications [17].

3.1 Numerical simulation method

The total pressure distortion, total temperature distortion, and swirl distortion should be combined to study the influences of combined distortions on the stability margin loss. The total pressure distortion, total temperature distortion, and swirl

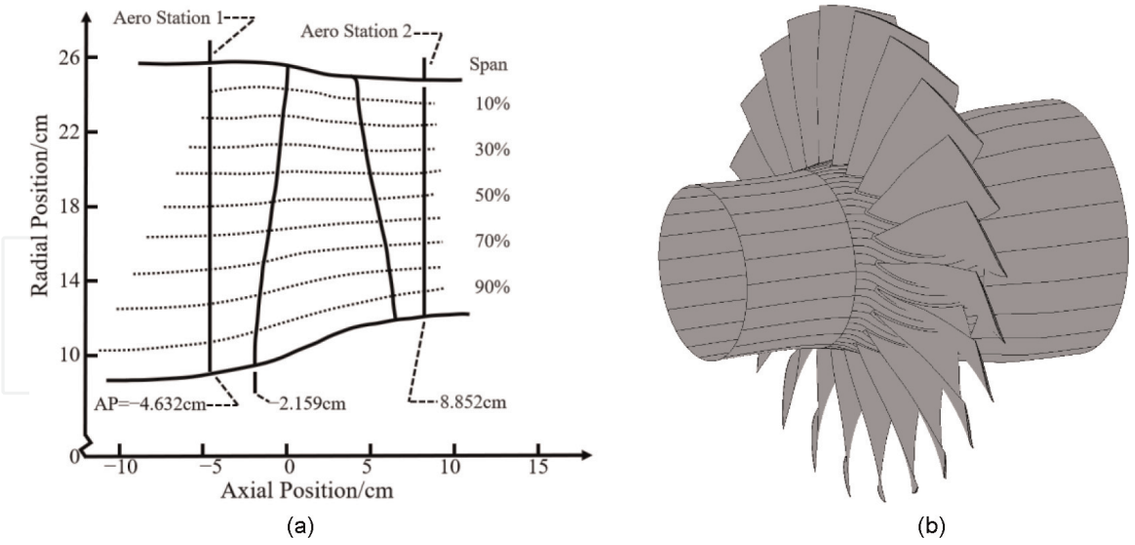

Figure 4.
NASA rotor 67. (a) Geometry definition including stations [16]. (b) 3D model.

Specification		Value
Number of rotor blades		22
Rotational speed [rpm]		16,043
Mass flow [kg/s]		33.25
Total pressure ratio		1.63
Rotor tip speed [m/s]		429
Tip clearance at a design speed [cm]		0.061
Inlet tip relative Mach Number		1.38
Rotor aspect ratio		1.56
Tip diameter [cm]	Inlet	51.4
	Exit	48.5
Hub-to-tip radius ratio	Inlet	0.375
	Exit	0.478

Table 1.
Basic specifications of NASA rotor 67 [17].

distortion in the actual distortion of the outlet section of the inlet duct obtained in aircraft outflow calculation results all exist at the same time and change with the outflow conditions. Therefore, it is impossible to directly obtain the flow conditions with/without the swirl distortion or different swirl distortions under the total pressure and total temperature distortion. The inlet boundary of the rotor in the internal flow calculation is the outlet section of the inlet duct in the outflow calculation. The gas parameters at the outlet section of the inlet duct obtained from the outflow calculation should be interpolated and combined to obtain the internal flow calculation boundary conditions with adjustable distortion parameters (see **Figure 5**).

The total pressure distortion parameter is taken as an example. When the total pressure distortion parameter on the outlet section of the inlet duct in outflow

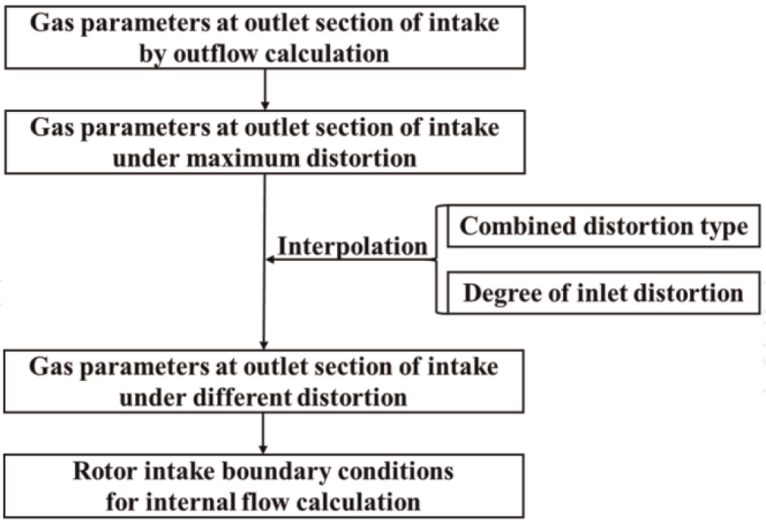

Figure 5.
Interpolation and combination process.

calculation results is the maximum, the total pressure at each node of the outlet section of the inlet duct under the corresponding working condition is taken as the reference value for pressure interpolations. Similarly, the reference values of the temperature interpolation and velocity-component interpolation can be obtained.

Table 2 shows the corresponding working conditions of the maximum values of each distortion parameter. The pressure, temperature, velocity components, and other gas parameters at each node are interpolated in turn and then combined to obtain the required rotor inlet boundary conditions of the internal-flow calculation according to the relative distortion degree and the combined distortion type in the designed calculation condition. Besides, the interpolation of calculated grid nodes is required because different calculated grids correspond to the external conditions when the total pressure distortion parameter, total temperature distortion parameter, and swirl distortion parameter are maximum.

3.2 Verification of the numerical simulation method

Calculate the performance of Rotor 67 under undistorted intake air by the CFD method, and compare it with the experiment results of Rotor 67 [16] to verify the numerical simulation method. **Figure 6** shows the comparison between the characteristic maps obtained by the CFD calculation and experiment results. The pressure-ratio characteristic line of CFD calculation results is lower than that of experiment results under same airflow, and the characteristic line of the efficiency is relatively consistent. The comparison results show that the numerical simulation method used in the work can better fit the actual working conditions, with reliability.

Distortion type	Maximum distortion parameter
Total pressure distortion	5.7540%
Total temperature distortion	18.7302%
Swirl distortion	0.185257

Table 2.
Corresponding working conditions of the maximum values of each distortion parameter.

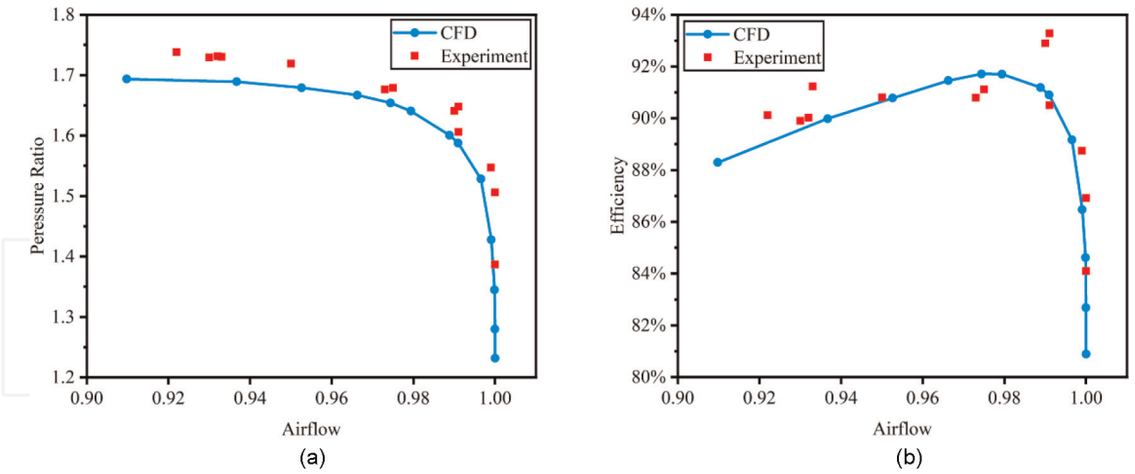

Figure 6.
Comparison of characteristics between CFD results and experiment results. (a) Total pressure ratio. (b) Efficiency.

4. Effect of pure distortions on aerodynamic stability of fans

4.1 Effect of the pure total pressure distortion on aerodynamic stability of fans

The distortion screens of variable solidity in the inlet duct block a 180° sector of the inlet annulus to generate the total pressure distortion of the compressor inlet. **Figure 7** shows typical circumferential profiles resulting from averaging the pressures on each rake. The total pressure profile reasonably approximates a 180° extent square wave at the compressor inlet, whereas the static pressure profile appears sinusoidal.

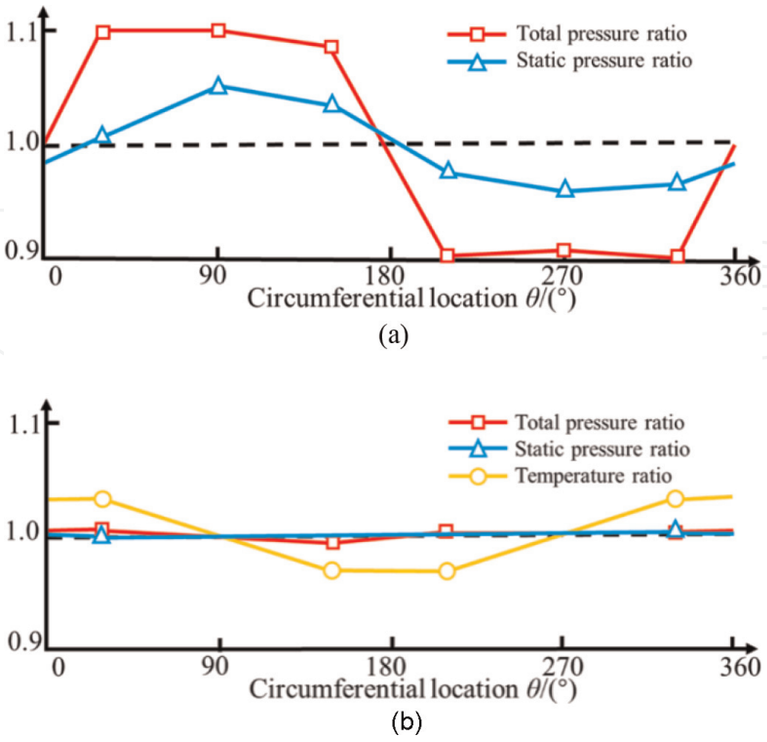

Figure 7.
Compressor profiles with the 180° circumferential pressure distortion at the 94% designed speed [18]. (a) Compressor inlet. (b) Compressor outlet.

The compressor-outlet profiles show very little circumferential variation in the total/static pressure; however, a total temperature distortion is evident. If the region of higher exit temperature is the result of the higher compression heat in the distorted sector, distorted flow rotates approximately 90° in the rotor-rotating direction passing from the low-pressure sector of the compressor inlet to the compressor outlet [18].

The effects of different distortion amplitudes (screen solidity) on the compressor-stall line are shown on the undistorted compressor map (see **Figure 8**). Each stall line is defined as the locus of stall points generated. P_d is the average of the pressure measurements on the rakes behind the distortion screen; P_{ud} is that in the undistorted region; P_{av} is the average of P_d and P_{ud}. The increased amplitude of the pressure distortion causes the stall line to move to lower pressure ratios. Also, the corrected rotor speed lines shift to the left or lower airflow for 93% of the corrected speed. The pressure distortion is not constant with airflow. The pressure distortion for screen "A" varies from 5% at 90% of the speed to 12% at the rated speed [18].

Figure 9 shows the effects of different total pressure distortions on $\Delta(PRS)$. Parameters $\Delta(PRS)_W$ and $\Delta(PRS)_N$, describing losses in the pressure ratio of stall at constant corrected airflow or a constant corrected speed, are used to evaluate the effects of flow distortions. $\Delta P/P$, the ratio of $\Delta(PRS)_N$ to the amplitude of the distortion, is approximately 0.60 and essentially independent of speeds with inlet pressure distortion alone. The ratio of $\Delta(PRS)_W$ to $\Delta P/P$, however, varies with speeds and amplitudes from 0.50 to 1.0, and the ratio is constant with the amplitude only at 93% of the corrected speed [18].

4.2 Effect of the pure total temperature distortion on aerodynamic stability of fans

The gaseous hydrogen burner in the inlet duct heats a 180° sector of the inlet annulus to generate the total temperature distortion of the compressor inlet. **Figure 10** shows typical circumferential profiles resulting from averaging the pressure and

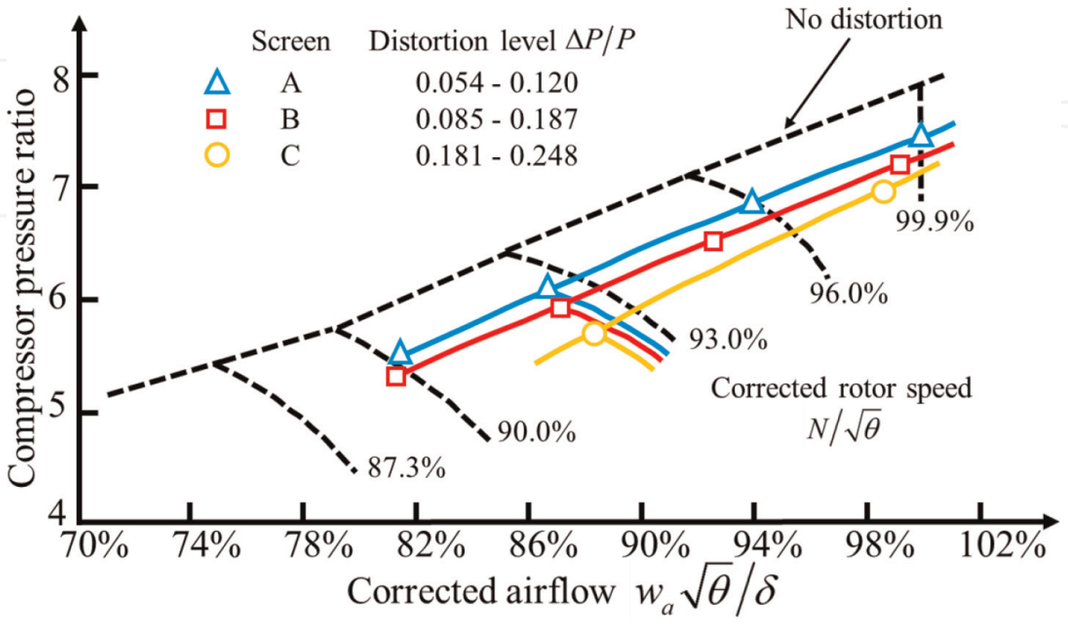

Figure 8.
Compressor map showing the effects of the 180° circumferential pressure distortion [18].

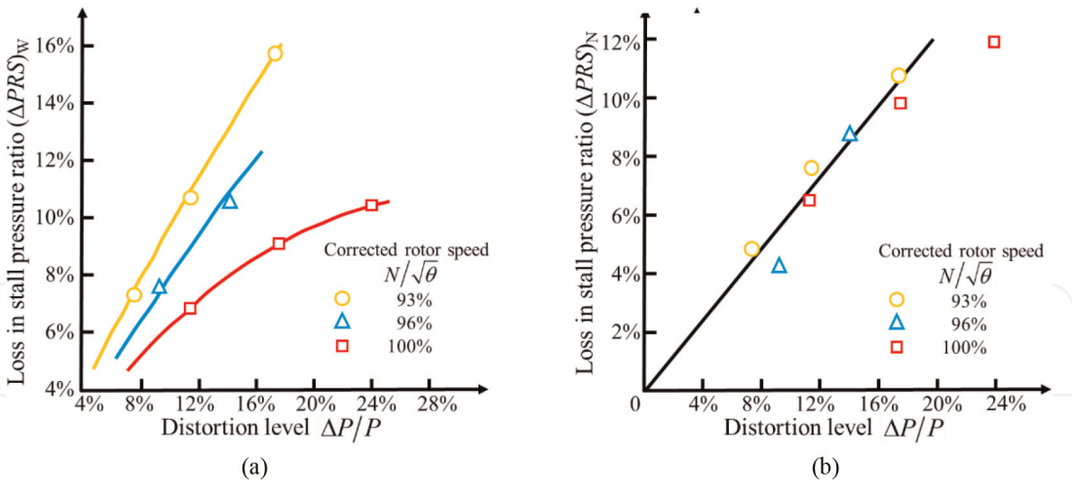

Figure 9.
Losses in the pressure ratio of stall for the 180°-extent inlet-pressure distortion [18]. (a) At constant corrected airflow. (b) At a constant corrected speed.

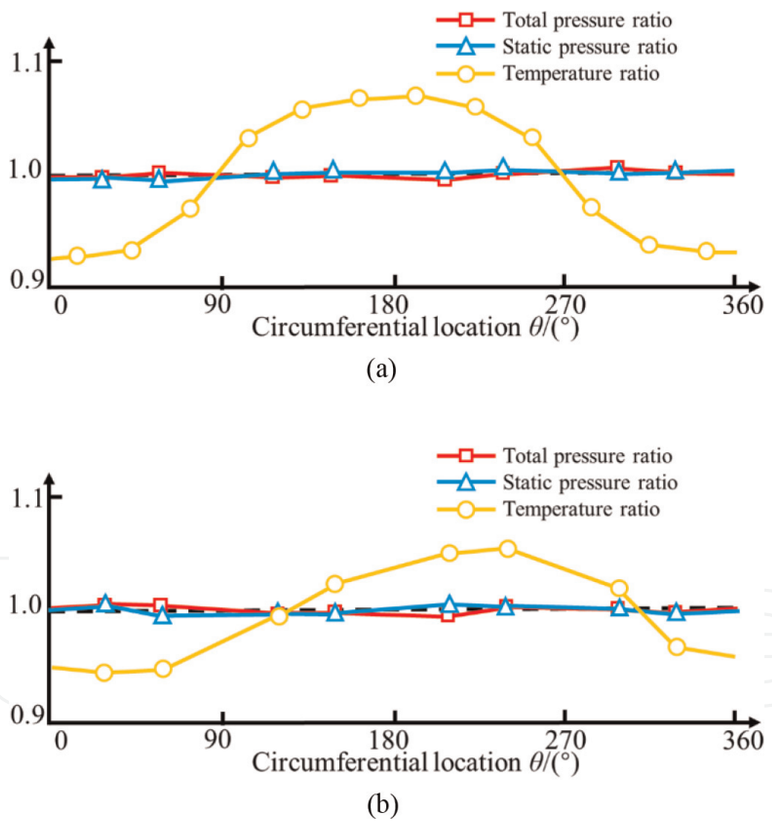

Figure 10.
Compressor profiles with the 180° circumferential temperature distortion at 96% of the designed speed [18]. (a) Compressor inlet. (b) Compressor outlet.

temperature on each rake. The temperature profile is more sinusoidal than the desired square wave pattern at the compressor inlet. The comparison of total temperature profiles of the compressor inlet and outlet indicates that the temperature distortion persists through the compressor with only a 29% reduction in the maximum amplitude, while the total pressure distortion is completely attenuated at the compressor outlet. Also, the peak temperature distortion rotates approximately 45° in the rotor-

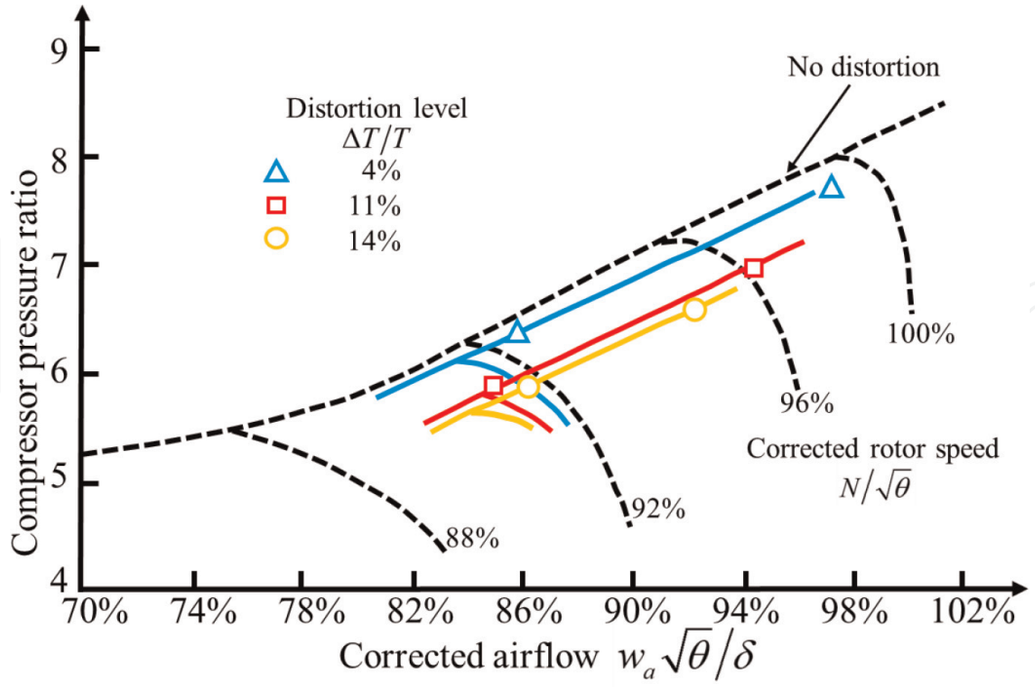

Figure 11.
Effects of the 180° circumferential temperature distortion [18].

rotating direction. There is little or no circumferential distortion of the total/static pressure associated with the temperature distortion at the compressor inlet or exit [18].

Effects on the stall line of different temperature distortions are presented on the undistorted compressor map (see **Figure 11**). T_d is the average of the temperature measurements in the heated region; T_{ud} is that in the undistorted region; T_{av} is the average of T_d and T_{ud}. The increased temperature distortion decreases the stall pressure ratio, while another effect is the decrease in the corrected rotor speed for a constant mechanical speed. The constant corrected speed lines also move to lower values of corrected airflow for 92% of the corrected speed [18].

Figure 12 shows the loss in the pressure ratio of stall evaluated at constant corrected airflow $\Delta(PRS)_W$ under different total temperature distortions. It is nearly

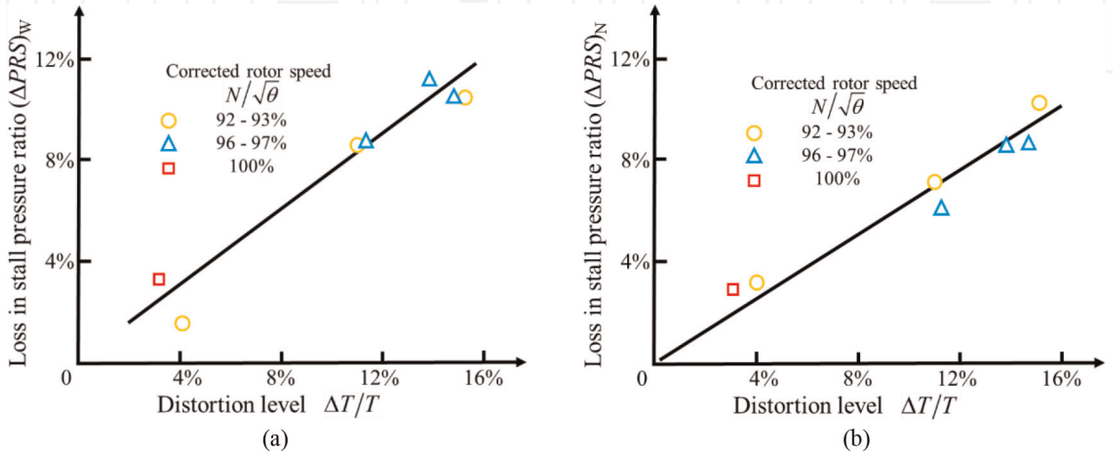

Figure 12.
Loss in the pressure ratio of stall for the 180°-extent temperature distortion [18]. (a) At constant corrected airflow. (b) At a constant corrected speed.

linear with amplitude $\Delta T/T$ of the temperature distortion, while the ratio of $\Delta(PRS)_W$ to $\Delta T/T$ is approximately 0.75. The loss in stall pressure ratio at constant corrected speed $\Delta(PRS)_N$ also appears to be linear, while the ratio of $\Delta(PRS)_N$ to $\Delta T/T$ is approximately 0.62 [18].

5. Effects of combined distortions on the aerodynamic stability of fans

The numerical simulation of binary combined distortions is performed. The stability margin loss of the rotor under different combined distortions is calculated to obtain the relationship between the stability margin loss and each distortion parameter.

5.1 Effect of the total pressure and swirl distortion on the aerodynamic stability of fans

The stability margin loss of the rotor increases under the total pressure and swirl distortion when the swirl and temperature distortion increases (see **Figure 13**). When the total pressure distortion increases under the low swirl distortion or decreases under the high swirl distortion, the stability margin loss of the rotor also increases. Binary linear regression is performed on the numerical simulation results, and the regression coefficient is about 91.0%.

The instability mechanism of the total pressure and swirl distortion can be sunnitized as follows. **Figure 14** shows the unwrapped blade-to-blade snapshots of the total pressure and velocity under the maximum stability margin loss at different spans. The speed in the distorted sector is lower than that in the clean sector at 99% of the span. The blockage phenomenon has spread from cascades to the front of cascades, and a protruding low-pressure region with a width of about 10 cascades forms in front of cascades. The cascades after the low-pressure region have obvious stall. Although the rotor is still blocked, the influence degree and range of blockage at 80% of the span are weaker than those at 99% of the span, and the low-pressure region in front of the cascade has been reduced to about 7 cascade widths.

The area of the protruding low-pressure region in front of the cascade has little change at 50% of the span, and blockage is no longer obvious. The number of stalled

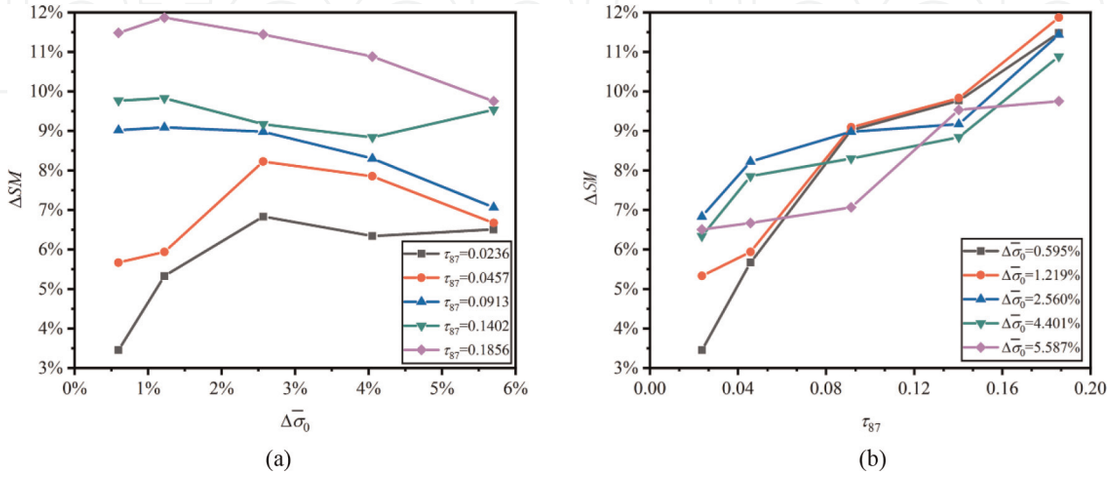

Figure 13.
Stability margin loss under the total pressure and swirl distortion. (a) Total pressure distortion parameters as the abscissa. (b) Swirl distortion parameters as the abscissa.

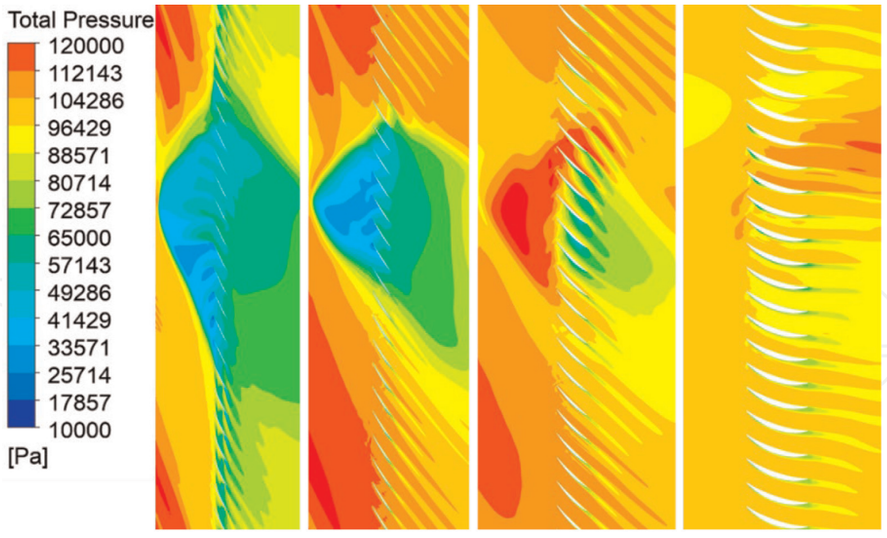

(a) Total pressure distribution

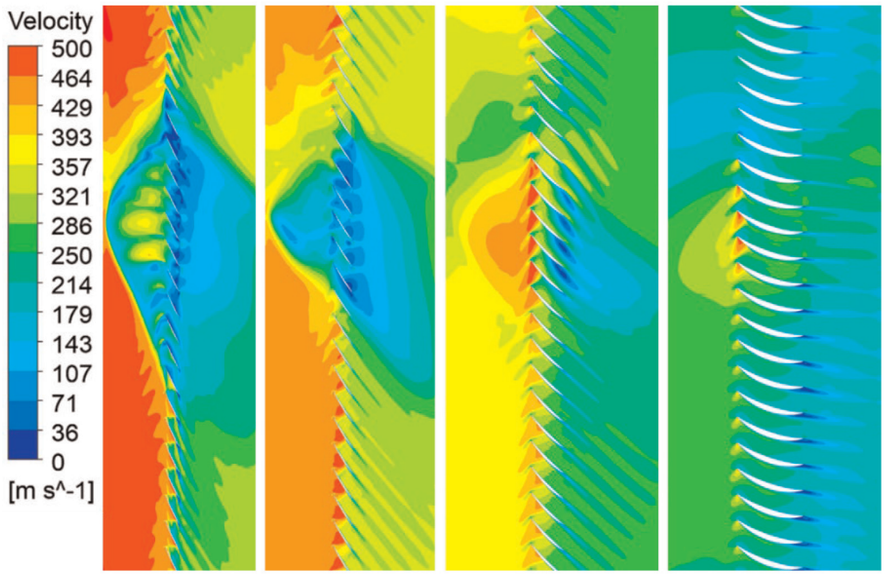

(b) Velocity distribution

Figure 14.
Different spans with a maximum stability margin loss under the total pressure and swirl distortion (from left to right: 99, 80, 50, and 10% of the span). (a) Total pressure distribution. (b) Velocity distribution.

cascades decreases, and the overall high-speed region appears at the cascade inlet. The protruding low-pressure region in front of the cascade is not obvious at 10% of the span, and flow in the rotor tends to be normal. Therefore, when the rotor is under the total pressure and swirl distortion, stall and blockage appear at the tip first and then gradually spread to the midspan and root of the hub.

5.2 Effects of the total temperature and swirl distortion on the aerodynamic stability of fans

The stability margin loss of the rotor increases under the total temperature and swirl distortion when the total temperature distortion decreases or the swirl distortion increases (see **Figure 15**). The binary linear regression is performed on the numerical simulation results, and the regression coefficient is about 93.0%.

The instability mechanism under the total temperature and swirl distortion is generally similar to that under the total pressure and swirl distortion. **Figure 16** shows unwrapped blade-to-blade snapshots of the total pressure and velocity under the maximum stability margin loss at different spans. The blockage phenomenon has spread from the cascades to the front of the cascades at 99% of the span, and a protruding low-pressure region covering the entire circumference has been formed in front of the cascade. Almost all cascades have serious stall phenomena. Although the rotor is still blocked, the influence degree and range of the blockage are weaker at 80%

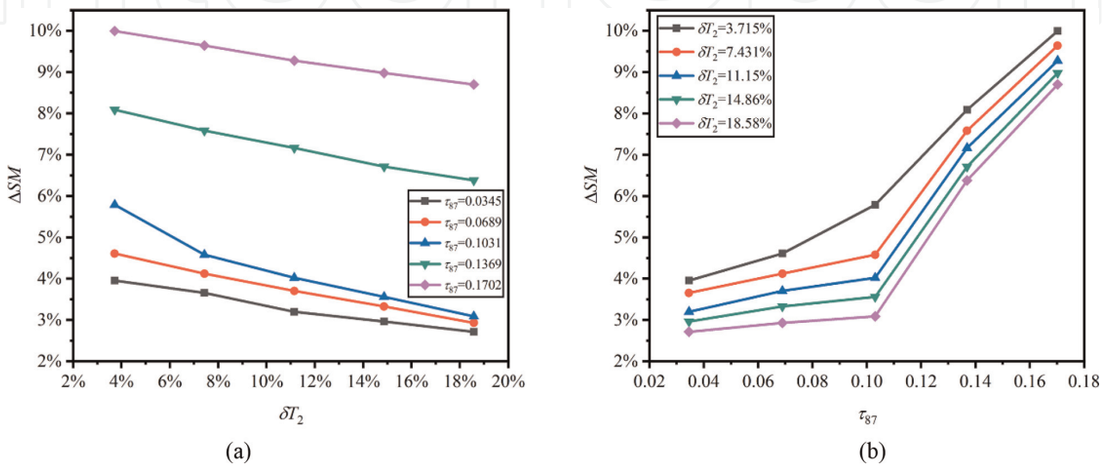

Figure 15.
Stability margin loss under the total temperature and swirl distortion. (a) Total temperature distortion parameters as the abscissa. (b) Swirl distortion parameters as the abscissa.

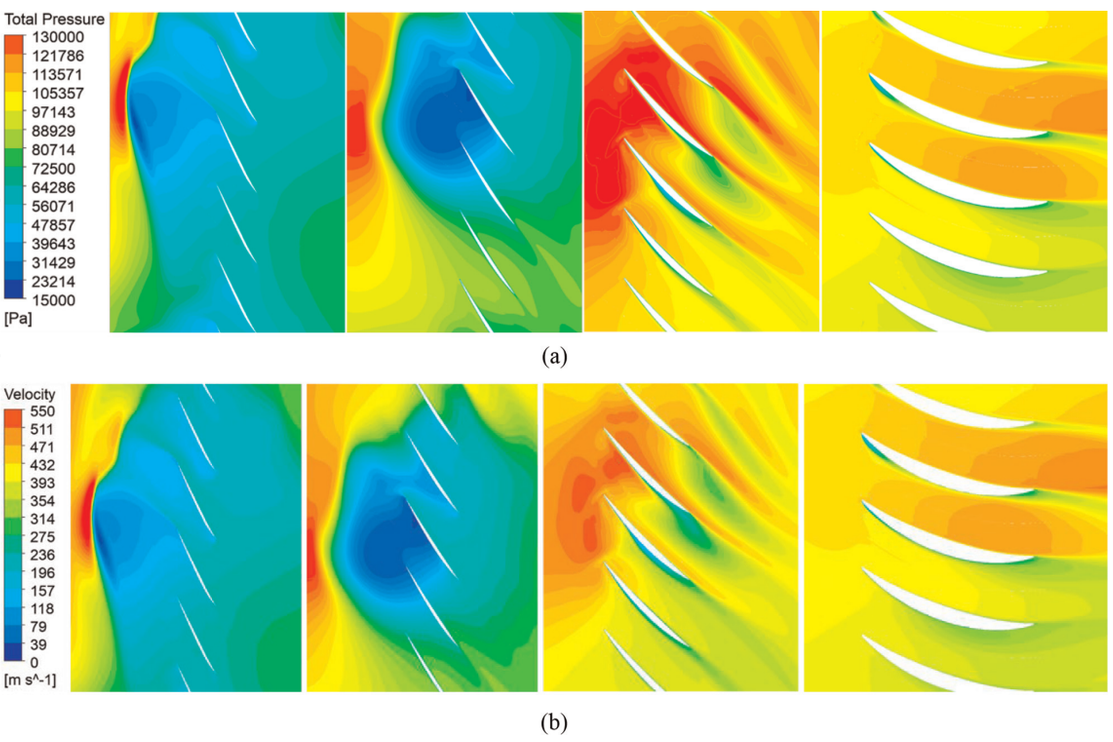

Figure 16.
Different span with a maximum stability margin loss under the total temperature and swirl distortion (from left to right: 99, 80, 50, and 10% of the span). (a) Total pressure distribution. (b) Velocity distribution.

of the span than those at 99% of the span. The low-pressure region in front of the cascade has been reduced to two stall cells, one is big and the other is small.

Flow tends to be normal in the lower blade-height plane, but some cascades still stall. Flow tends to be normal at the span closer to the hub, but some cascades still stall. Therefore, when the rotor is under the total temperature and swirl distortion, stall and blockage appear at the tip first and then gradually spread to the midspan and root of the hub.

5.3 Effect of the total pressure and total temperature distortion on the aerodynamic stability of fans

The stability margin loss of the rotor increases under the total pressure and total temperature distortion when the total pressure distortion increases or the total temperature distortion decreases (see **Figure 17**). Binary linear regression is performed on the numerical simulation results, and the regression coefficient is about 84.1%.

The instability mechanism under the total pressure and total temperature distortion is generally similar to that under the total pressure and swirl distortion. **Figure 18** shows unwrapped blade-to-blade snapshots of the total pressure and velocity under the maximum stability margin loss at different spans. When the rotor is under the total pressure and total temperature distortion, stall and blockage appear at the tip first and then gradually spread to the midspan and root of the hub.

5.4 Functional relationship between distortion parameters and the aerodynamic stability of fans

First of all, the calculated examples are supplied using a uniform test design to increase the generality, universality, and reliability of the calculation results. Secondly, the mathematical relations between the stability margin loss and distortion parameters are derived and used as the basis for the next calculation and analysis to strengthen the logic of the calculation and analysis (**Figure 19**).

The changes in the velocity triangle before and after the swirl distortion and mathematical approximation show that stability margin loss ΔSM and swirl distortion

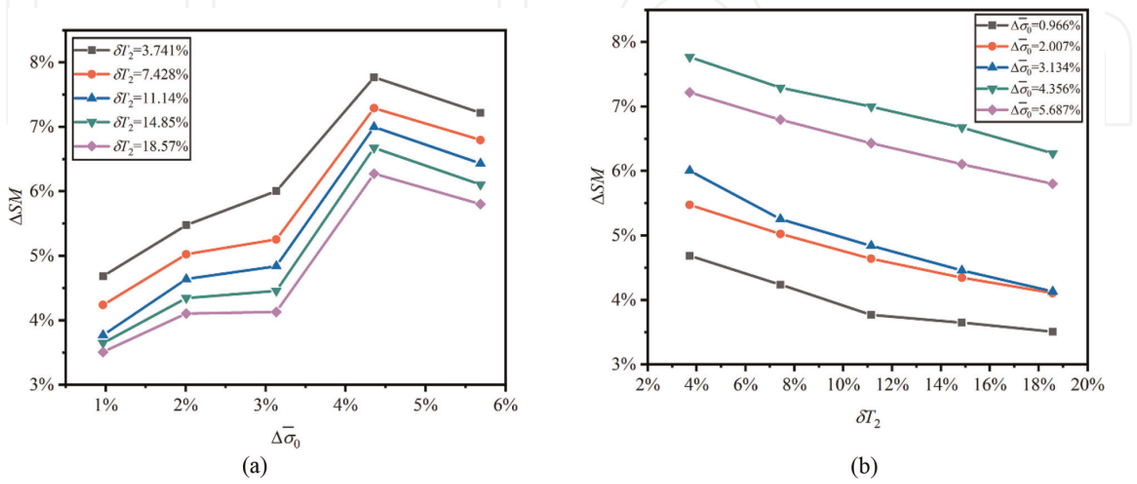

Figure 17.
Stability margin loss under the total pressure and total temperature distortion. (a) Total pressure distortion parameters as the abscissa. (b) Total temperature distortion parameters as the abscissa.

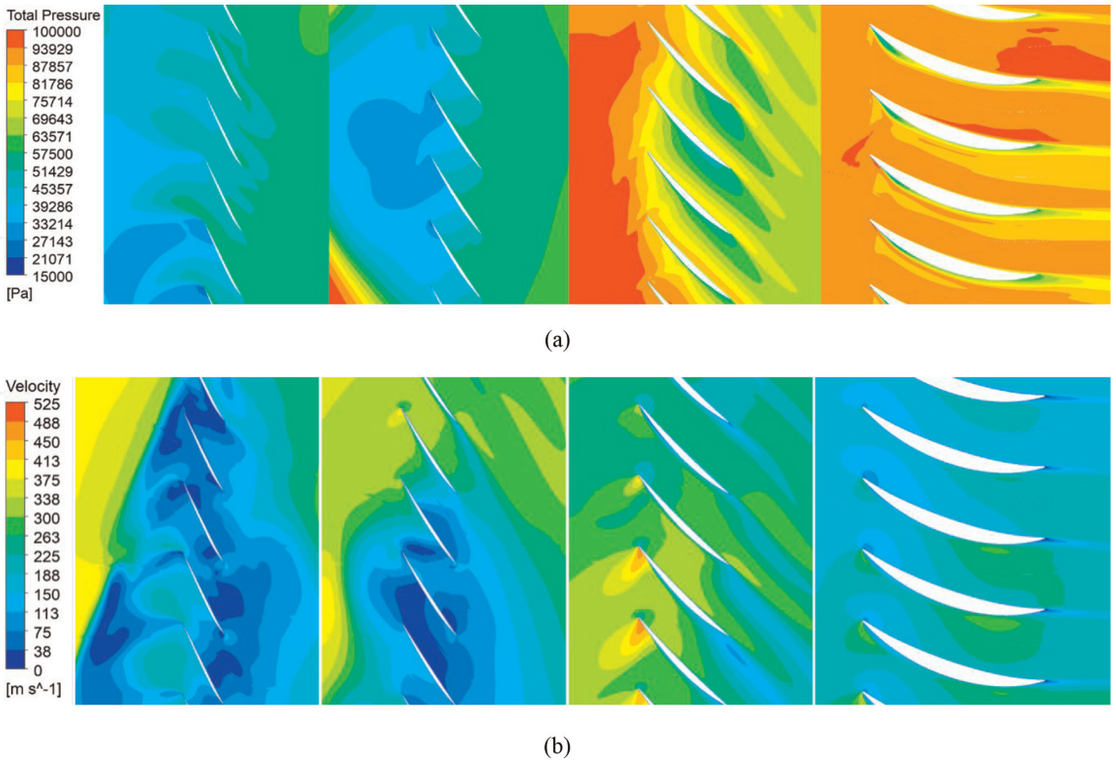

Figure 18.
Maximum stability margin loss under the total pressure and total temperature distortion at different spans (from left to right: 99, 80, 50, and 10% of the span). (a) Total pressure distribution. (b) Velocity distribution.

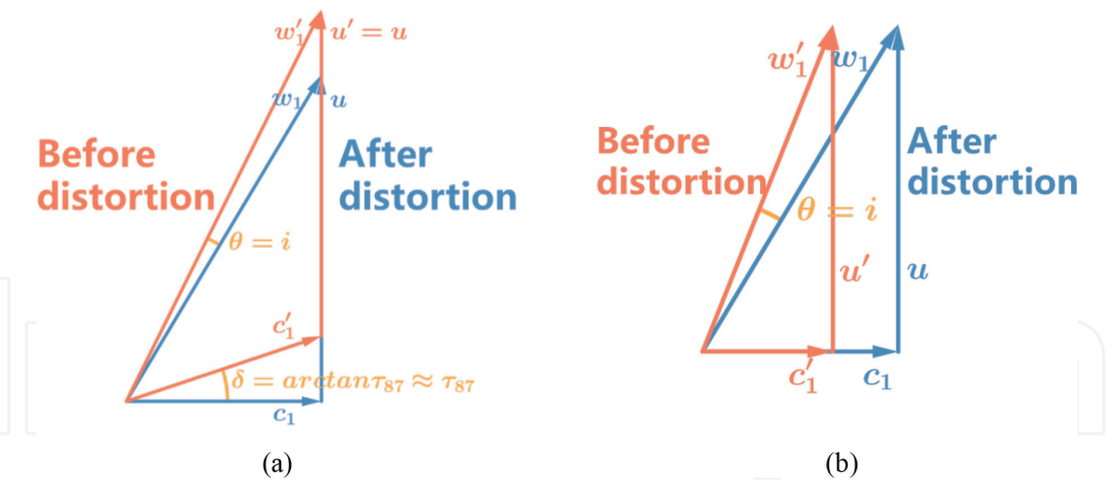

Figure 19.
Velocity triangles before and after the distortion. (a) Swirl distortion. (b) Total temperature distortion.

parameter $\overline{\tau}_{87}$ have an approximate quadratic relationship when loss coefficient $\overline{\omega}$ has an approximate quadratic relationship with attack angle i and an approximately linear relationship with stability margin SM (see Eq. (6)).

Similarly, the changes in the velocity triangle before and after the total temperature distortion and mathematical approximation show that stability margin loss ΔSM and total temperature distortion parameter $\delta T_{2\mathrm{FAV}}$ have an approximately quartic relationship (see Eq. (7)). Besides, stability margin loss ΔSM and total pressure distortion parameter $\Delta\overline{\sigma}_0$ have an approximately linear relationship (see Eq. (8)). The

approximate error derived from the above mathematical relationship is within the acceptable range through mathematical verification.

$$\Delta SM_\tau \sim \overline{\omega} \sim i^2 \sim \tau_{87}^2 \tag{6}$$

$$\Delta SM_\tau \sim \overline{\omega} \sim i^2 \sim \left(\frac{\Delta T}{T}\right)^4 \tag{7}$$

$$\Delta SM_p \sim \overline{\omega} \sim \frac{\Delta p}{p} \tag{8}$$

According to the numerical simulation results including the ternary combined distortion examples, linear regression fitting is carried out based on the approximate mathematical relationship between the stability margin loss and each distortion parameter derived above. The obtained fitting equation is used as the prediction model of the stability margin loss of fans based on combined distortion parameters (see Eq. (9)).

$$\Delta SM = tr(AX) + B \tag{9}$$

where

$$A = \begin{bmatrix} a_1 & 0 & 0 & 0 \\ a_2 & a_4 & a_6 & a_7 \\ a_3 & a_5 & 0 & 0 \end{bmatrix} \tag{10}$$

$$X = \begin{bmatrix} \Delta\overline{\sigma}_0 & \delta T_2 & \tau_{87} \\ \Delta\overline{\sigma}_0{}^2 & \delta T_2{}^2 & \tau_{87}{}^2 \\ \Delta\overline{\sigma}_0{}^3 & \delta T_2{}^3 & \tau_{87}{}^3 \\ \Delta\overline{\sigma}_0{}^4 & \delta T_2{}^4 & \tau_{87}{}^4 \end{bmatrix} \tag{11}$$

$$B = a_0 \tag{12}$$

Table 3 shows the parameter values in the prediction model.

Compared with the CFD calculation results, the error of the prediction model is generally within ±3.1%; the average of the absolute value of the error is 0.801%; the median of the absolute error value is 0.610%. To sum up, the prediction results are generally good.

Parameter No.	Parameter value
0	0.058579
1	0.363079
2	−0.033317
3	−0.124045
4	−4.00817
5	2.11732
6	31.9687
7	−71.91360

Table 3.
Parameter values of the prediction model.

Figure 20 shows the prediction results. Scattered points are CFD calculation data, and the 3D counter is the prediction result. The prediction model has a good prediction effect and can be used as a prediction tool for the stability margin loss.

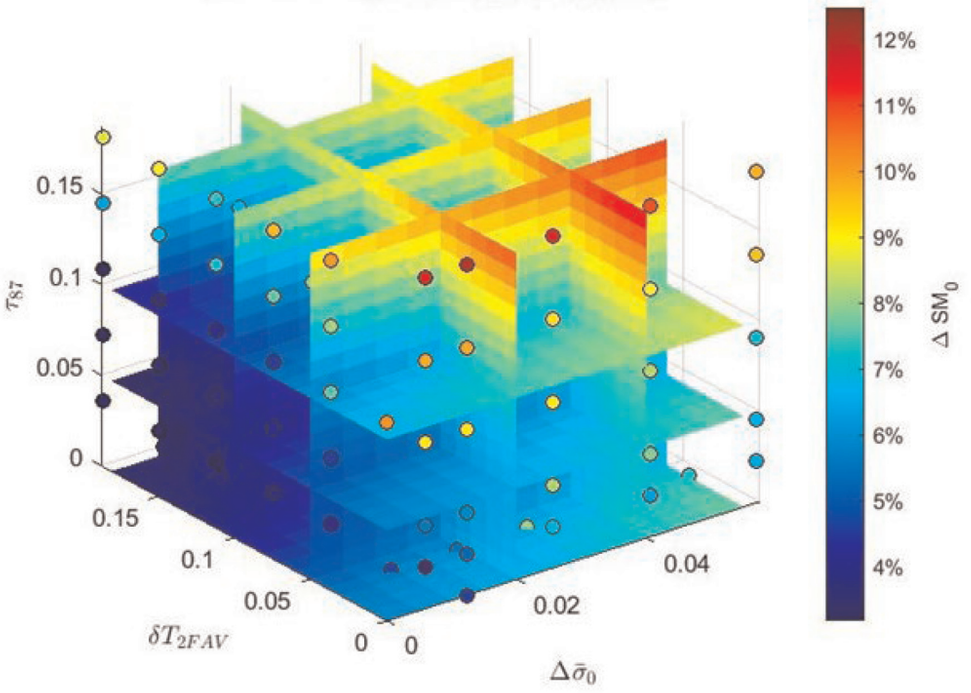

(a)

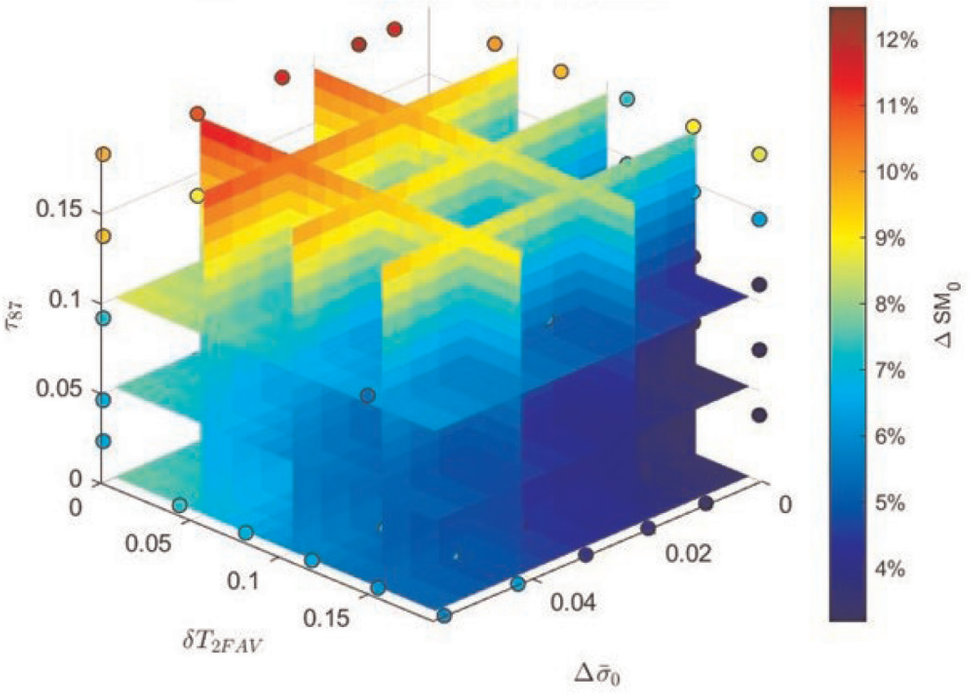

(b)

Figure 20.
Prediction of the stability margin loss under the total pressure, total temperature, and swirl distortion based on the prediction model. (a) View of the low-total-pressure and low-total-temperature distortion. (b) View of the high-total-pressure and high-total-temperature distortion.

6. Conclusions

The 3D CFD numerical simulation was utilized in the work. First, the numerical simulation method was verified to ensure the credibility of the results. Then the influences of combined distortions on the aerodynamic stability of fans were numerically calculated. The following conclusions are obtained:

1. The stability margin loss of the rotor increased under the total pressure and swirl combined distortion when the swirl and temperature distortion increased. When the total pressure distortion increased under the low swirl distortion or decreased under the high swirl distortion, the stability margin loss of the rotor also increased. The instability mechanism showed that stall and blockage appeared at the tip first and then gradually spread to the midspan and root of the hub when the rotor was under total pressure and swirl distortion.

2. The stability margin loss of the rotor increased under the total temperature and swirl distortion when the -distortion decreased or the swirl distortion increased. The instability mechanism under the total temperature and swirl distortion was generally similar to that under the total pressure and swirl distortion.

3. The stability margin loss of the rotor increased under the total pressure and total temperature distortion when the total pressure distortion increased or the total temperature distortion decreased. The instability mechanism under total temperature and total temperature combined distortion was generally similar to that under total pressure and swirl combined distortion.

4. A prediction model of the stability margin loss of fans based on combined distortion parameters was established through linear regression fitting and an approximate mathematical relationship between the stability margin loss and each distortion parameter. The model was used for verification, and the error was within ±3.1% compared with CFD calculation results. The model has good prediction ability and can be used as a prediction tool for stability margin losses.

Author details

Xu Quanyong[1*], Wu Honghu[2] and Hou Anping[2]

1 Tsinghua University, Beijing, China

2 Beihang University, Beijing, China

*Address all correspondence to: xqybuaa@163.com

References

[1] Braithwaite WM, Soeder RH. Combined pressure and temperature distortion effects on internal flow of a turbofan engine. Journal of Aircraft. 1980;**17**(7):468-472

[2] Soeder RH, Mehalic CM. Effect of Combined Pressure and Temperature Distortion Orientation on High-Bypass-Ratio Turbofan Engine Stability. Technical report, NASA TM-83771. Cleveland, Ohio, USA: NASA; 1984

[3] Mehalic CM. Effect of spatial inlet temperature and pressure distortion on turbofan engine stability. In: AIAA/ASME/SAE/ASEE 24th Joint Propulsion Conference. Boston, Massachusetts, USA: AIAA; 1988. Paper number AIAA-88-3016

[4] Davis M Jr. Parametric investigation into the combined effects of pressure and temperature distortion on compression system stability. In: AIAA/ASME/SAE/ASEE 27th Joint Propulsion Conference. Sacramento, California, USA: AIAA; 1991. Paper number AIAA-91-1895

[5] Davis MW Jr, Cousins WT. Evaluating complex inlet distortion with a parallel compressor model: Part 2—Applications to complex patterns. In: ASME Turbo Expo 2011. Vancouver, British Columbia, Canada: ASME; 2011. Paper number GT2011-45068

[6] Frohnapfel DJ, Ferrar AM, Bailey JM, O'Brien WF, Lowe KT. Measurements of fan response to inlet total pressure and swirl distortions produced by boundary layer ingesting aircraft configurations. In: 54th AIAA Aerospace Sciences Meeting. San Diego, California, USA: AIAA; 2016. Paper number AIAA-2016-0533

[7] Huang SZ. A numerical study in effect of combined pressure and temperature distortion on engine stability. Gas Turbine Experiment and Research. 2002; **15**(01):28-32 (in Chinese)

[8] Ye W, Hou MJ, Zhou ZW. Numerical study on the effects of pressure and temperature distortion of an engine. Gas Turbine Experiment and Research. 2007; **20**(04):41-44+21 (in Chinese)

[9] Xie YP, Liu YQ, Pan BJ. Aerodynamic calculation method of engine stability under actual inlet condition. Journal of Aerospace Power. 2019;**34**(04):804-812 (in Chinese)

[10] Pearson H, McKenzie AB. Wakes in axial compressors. Journal of the Royal Aeronautical Society. 1959;**63**(583): 415-416

[11] Reid C. The response of axial flow compressors to intake flow distortion. In: Gas Turbine Conference & Products Show. Cleveland, Ohio, USA: ASME; 1969. Paper number 69-GT-29

[12] Mazzawy RS. Multiple segment parallel compressor model for circumferential flow distortion. Journal of Engineering for Gas Turbines Power. 1977;**99**(2):288-296

[13] Davis MW Jr, Cousins WT. Evaluating complex inlet distortion with a parallel compressor model: Part 1—Concepts, theory, extensions, and limitations. In: ASME Turbo Expo 2011. Vancouver, British Columbia, Canada: ASME; 2011. Paper number GT2011-45067

[14] SAE International. Inlet Total-Pressure-Distortion Considerations for Gas-Turbine Engines. Warrendale,

Pennsylvania, USA: Standard No. AIR1419 Revision C; 2017

[15] Peng CY, Ma JJ, Yin JF. Measurement of inlet swirls in flight. Journal of Propulsion Technology. 1994; **04**:8-13 (in Chinese)

[16] Strazisar AJ, Wood JR, Hathaway MD, Suder KL. Laser Anemometer Measurements in a Transonic Axial-Flow Fan Rotor. Technical report, NASA-TP-2879. Cleveland, Ohio, USA: NASA; 1989

[17] Arima T, Sonoda T, Shirotori M, Tamura A, Kikuchi K. A numerical investigation of transonic axial compressor rotor flow using a low-Reynolds-number k–ε turbulence model. Journal of Turbomachinery. 1999;**121**(1): 44-58

[18] Braithwaite WM, Graber EJ Jr, Mehalic CM. The effects of inlet temperature and pressure distortion on turbojet performance. In: AIAA/SAE 9th Propulsion Joint Specialists Conference, Las Vegas. Nevada, USA: NASA TM-X-71431; 1973